J Solid State Electrochem (2001) 5: 450–458
DOI 10.1007/s100080000188

ORIGINAL PAPER

**Alexander Nemudry · Andrey Rogatchev
Igor Gainutdinov · Robert Schöllhorn**

Reactivity of the perovskite system $Ca_{1-x}Sr_xFeO_{2.5}$ in topotactic electrochemical oxidation at ambient temperature

Received: 3 September 2000 / Accepted: 15 November 2000 / Published online: 11 July 2001

Abstract Electrochemical galvanostatic oxidation of strontium-substituted $CaFeO_{2.5}$ at room temperature in an alkaline electrolyte is described. Samples with nominal composition $Ca_{1-x}Sr_xFeO_{2.5}$ were completely oxidized to the cubic perovskite at $x \geq 0.25$. The substitution at this level is accompanied by phase separation with formation of Ca- and Sr-enriched microdomains and a sharp increase in the reactivity of the matrix. The study confirms the phenomenological model which describes an anomalous rapid oxidation process in perovskites for such a low temperature as a result of long-range fast oxygen transport along microdomain walls, followed by slow diffusion over short distances in defect-free domains.

Keywords Perovskites · Electrochemical oxygen intercalation · Microdomains

Introduction

It has been shown earlier that brownmillerite-type compounds $SrMO_{2.5}$ (M = Fe, Co) are able of undergoing electrochemical oxygen intercalation with the formation of perovskites $SrMO_3$ in alkaline electrolytes at room temperature [1, 2, 3, 4]. We have suggested earlier that the unusually high reactivity of brownmillerites at low temperatures is related to the presence of high concentrations of extended defects in the structure of the initial compounds and intermediate products of the oxidation. These defects are defined in part by the prehistory of the sample but can arise also during intercalation. We assume these defects to be responsible for the low activation energy transport of oxygen [3, 4]. A phenomenological model has been proposed which describes the unusual high reactivity of brownmillerites at low temperatures as a result of long-range fast oxygen transport along extended defect channels followed by slow diffusion into defect-free domains [5, 6].

In order to check the proposed model, we have selected calcium ferrite ($CaFeO_{2.5}$), which belongs to the brownmillerite-type structure, like $SrFeO_{2.5}$, but exhibits a high degree of lattice order and is characterized by extremely low reactivity with respect to oxidation. Thus, oxidation of calcium ferrite with the formation of $CaFeO_3$ is achieved in girdle-type high-pressure apparatus at 1000 °C and $P_{O_2} = 2$ GPa [7]. According to the model proposed by us, the introduction of high concentrations of extended defects into the lattice of $CaFeO_{2.5}$ should increase its reactivity towards electrochemical oxidation at low temperature.

For inducing disorder in the lattice of $CaFeO_{2.5}$, we decided to use isomorphic substitution of Ca by Sr. We hoped that the similarity of the $CaFeO_{2.5}$ and $SrFeO_{2.5}$ structures, but the differences in unit cell volume and oxygen affinity, would allow us to obtain phase separation with microdomain formation which would permit us to achieve, at a definite substitution degree, a high concentration of extended defect channels (domain walls, anti-phase boundaries, stacking faults, etc.), to decrease the size of defect-free domains, thus realizing the necessary conditions for the proposed model.

Experimental

$Ca_{1-x}Sr_xFeO_{2.5}$ samples were prepared by standard solid state techniques. Stoichiometric amounts of $CaCO_3$, $SrCO_3$ and Fe_2O_3

Presented at the international conference "Solid State Chemistry 2000", 3–8 September 2000, Prague, Czech Republic

A. Nemudry (✉) · A. Rogatchev · I. Gainutdinov
Institute of Solid State Chemistry and Mechanochemistry,
Siberian Branch of the Russian Academy of Science,
Kutateladze 18, 630128 Novosibirsk, Russia
E-mail: nemudry@solid.nsk.su
Tel.: +7-3832-363832
Fax: +7-3832-322847

R. Schöllhorn
Institut für Anorganische und Analytische Chemie,
Technische Universität Berlin, 10623 Berlin, Germany

(analytical grade) were ground and calcined in air at 900 °C for 12 h. The samples were pelletized and heated in air at temperatures of 1200 °C (24 h), 1000 °C (12 h) and quenched thereafter in liquid N_2. To remove the rest of the oxygen excess, the pellets of $Ca_{1-x}Sr_xFeO_{2.5+y}$ were placed into a quartz ampoule heated at 1000 °C under dynamic vacuum (10^{-2} Torr) for 6 h and quenched under vacuum in liquid N_2.

The oxygen stoichiometry was determined by routine iodo metry: 20–30 mg of the sample and 1.5 g KI were dissolved in 50 mL of 0.7 M HCl under a N_2 flow, and the I_2 formed was titrated with 0.02 N sodium thiosulfate.

Powder X-ray diffraction data were measured with a Siemens D 5000 diffractometer using Cu K_α radiation.

Electrochemical experiments were performed at room tem perature in galvanostatic mode (three-electrode cell, 1 M KOH electrolyte) with working electrodes of polycrystalline material (20–50 mg) pressed into Pt grids along with 1 wt% of Teflon and 15–20 wt% of acetylene black.

Mössbauer spectroscopy measurements were carried out by the conventional constant acceleration technique at room temperature. The isomer shift data are given relative to the isomer shift of α-iron.

Electron diffraction and microscopy studies were performed on a JEM-100CX (accelerating voltage 100 kV, point resolution 4.5 Å). Bright (BF) and dark (DF) field image regimes were used, as well as selected area electron diffraction (SAED). The samples were ground in an agate mortar, and then suspensions in alcohol were prepared. A suspension was deposited onto amorphous hollow carbon films 200–300 Å thick.

Results

The results of iodometric titration and Mössbauer data of $Ca_{1-x}Sr_xFeO_{2.5}$ samples after their synthesis and vacuum treatment followed by quenching in liquid N_2 are presented in Table 1. These data show that, in all the samples, the oxygen stoichiometry is (within the experimental error given in parentheses) close to the ideal value for brownmillerite-type compounds. The Mössbauer spectra of the samples contain two components corresponding to Fe^{3+} in octahedral (1) and tetrahedral (2) sites of the brownmillerite structure. The table shows the parameters of the components (in mm/s). H is the splitting due to the magnetic field, δ is the chemical shift (with respect to α-Fe), G is the linewidth, Q is the quadrupole splitting. The component ratio (%) agrees with the data calculated from the iodometric titration within experimental error. Figure 1 shows X-ray diffraction patterns of $Ca_{1-x}Sr_xFeO_{2.5}$ samples. All reflections of the samples obtained can be indexed on the basis of a brownmillerite orthorhombic unit cell related to the cubic perovskite subcell by $a_c\sqrt{2} \times 4a_c \times a_c\sqrt{2}$.

Figure 2 shows the evaluation of the X-ray diffraction data. According to Fig. 2a, Ca replaced by Sr leads to a continuous change in the unit cell parameters (reduced parameters are shown in Fig. 2a) which is characteristic for solid solutions (Vegard's rule). For $x = 0.5$ the X-ray diffraction pattern exhibits, however, two sets of reflections with lattice parameters close to $Ca_{0.3}Sr_{0.7}FeO_{2.5}$ and $Ca_{0.7}Sr_{0.3}FeO_{2.5}$, which is evidence for the presence of a miscibility gap within the range $0.3 < x < 0.7$. A further increase in the Sr content of the samples ($x \geq 0.7$) is again accompanied by a continuous increase of the parameters. Thus, the X-ray data show that for the region with $0 < x < 0.3$ and $0.7 < x < 1$, the solid solutions $Ca_{1-x}Sr_xFeO_{2.5}$ exist.

Starting from the pure ternary phases, it can be seen from Fig. 2b that substitution by Ca or Sr leads to substantial broadening of the X-ray lines. Figure 2c shows the results of coherence length calculations according to the physical width for two sets of multiple reflections, (020–080) and (101–202), taking account of lattice strain. A $CaFeO_{2.5}$ sample obtained by prolonged annealing at 1000 °C followed by slow cooling was used as a standard for calculations of coherence length and lattice strain. In all cases, lattice strain was about 10^{-5}. One can see that the drop of coherence length occurs more sharply in the [010] direction, especially within the range $0 < x < 0.3$. As it is known that the coherence length is related to imperfections of the crystal lattice, the nature of the imperfections which exist in the $Ca_{1-x}Sr_xFeO_{2.5}$ samples was studied by electron microscopy.

Electron microscopy studies

Electron microscopy studies of $Ca_{1-x}Sr_xFeO_{2.5}$ samples showed that different nominal composition ranges ($0 < x < 0.3$, $0.3 < x < 0.7$ and $0.7 < x < 1$) were characterized by specific types of defects. We will discuss here first the pure ternary phases and subsequently the quaternary phases.

$CaFeO_{2.5}$

The sample is characterized by a high degree of ordering in the crystal lattice. However, we also observed crystal

Table 1 Oxygen stoichiometry and Mössbauer data[a] of $Ca_{1-x}Sr_xFeO_{2.5}$ samples

Composition and oxygen stoichiometry of the samples	H_1	δ_1	G_1	Q_1	H_2	δ_2	G_2	Q_2	$\%_1$	$\%_2$
$SrFeO_{2.49(1)}$	15.2	0.372	0.36	–0.31	12.8	0.16	0.37	0.29	50	50
$Ca_{0.2}Sr_{0.8}FeO_{2.51(1)}$	16.4	0.385	0.406	–0.35	13.8	0.19	0.5	0.325	45.9	54.0
$Ca_{0.3}Sr_{0.7}FeO_{2.50(1)}$	14.5	0.341	0.427	–0.294	12.5	0.176	0.491	0.296	49.2	50.7
$Ca_{0.5}Sr_{0.5}FeO_{2.49(1)}$	16.5	0.372	0.464	–0.304	13.9	0.179	0.526	0.34	47.6	52.3
$Ca_{0.7}Sr_{0.3}FeO_{2.50(1)}$	16.7	0.373	0.423	–0.31	14.1	0.188	0.412	0.367	48.7	51.2
$Ca_{0.75}Sr_{0.25}FeO_{2.49(1)}$	16.6	0.372	0.385	–0.301	14.0	0.19	0.435	0.372	47.2	52.7
$CaFeO_{2.49(1)}$	16.4	0.37	0.36	–0.301	13.4	0.19	0.36	0.36	50	50

[a]Subscripts 1 and 2 in Mössbauer parameters correspond to octahedral and tetrahedral components, respectively

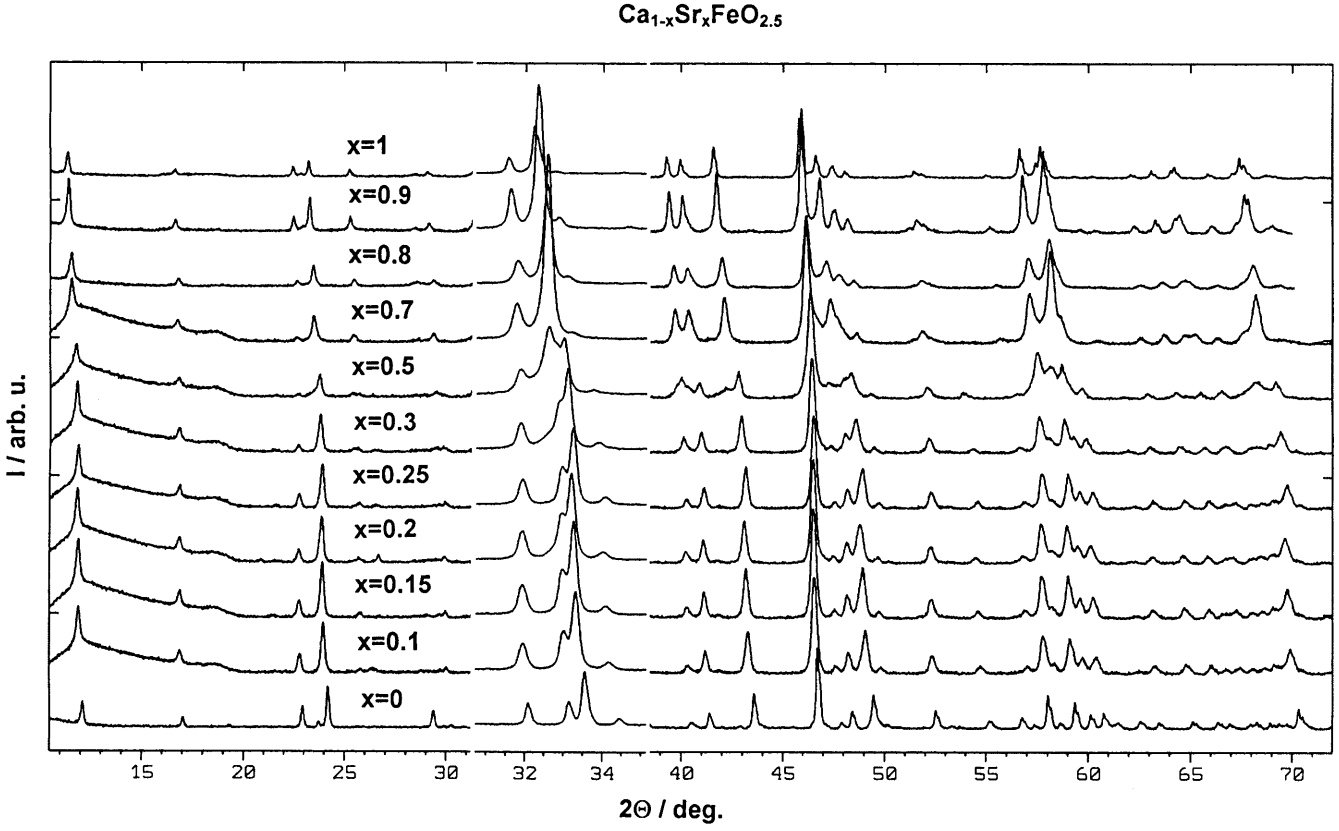

Fig. 1 X-ray diffraction patterns of $Ca_{1-x}Sr_xFeO_{2.5}$ samples

particles with twin boundaries in this sample. These boundaries are parallel to (010), their length is comparable to the crystal size and the shortest distances between neighbouring boundaries is in the order of 10^2–10^3 Å. Figure 3 shows a BF micrograph of a $CaFeO_{2.5}$ crystal edge. One can see rather smooth edge extinction contours simulating the relief of the external surface, which depicts the rather perfect character of the crystal lattice.

$SrFeO_{2.5}$

For this sample, we also observed particles containing twins which were similar to those found in $CaFeO_{2.5}$ samples. However, for the $SrFeO_{2.5}$ particles a clearly exhibited two-dimensional character of the electron microdiffraction with strong streaking of the reflections of the $0k0$ type along the b^* direction of the reciprocal lattice is typical (Fig. 4). Earlier we have shown that this phenomenon is connected with the presence of high concentrations of "stacking faults" in alternating octahedral and tetrahedral layers of brownmillerite [4]. Distortion of the alternation order can lead to the occurrence of different polytypes [8]. Altogether, the absence of point satellites in the vicinity of the major reflections of the SAED images points to the fact that the crystals do not contain polytype phase interlayers thicker than 20 Å.

Stacking faults can be clearly seen in the TEM images of the particles, with the [010] direction perpendicular to the direction of the electron beam. This is most obvious in DF images obtained in streaking reflections (Fig. 4b).

$Ca_{1-x}Sr_xO_{2.5}$ ($x = 0.3, 0.5, 0.7$)

We have selected the samples with these nominal compositions because they provide illustrations most clearly of the specific types of defects characteristic of the composition ranges which can be divided, on the basis of X-ray data, into one-phase regions of solid solutions of Ca in $SrFeO_{2.5}$ ($1 < x < 0.7$) and of Sr in $CaFeO_{2.5}$ ($0 < x < 0.3$) and a two-phase region ($0.3 < x < 0.7$).

For samples with nominal composition $Ca_{0.5}Sr_{0.5}O_{2.5}$, it is typical that Ca- and Sr-enriched microdomains are formed as a result of phase separation, which had been observed earlier during X-ray diffraction studies (Figs. 1, 2). Figure 5a shows a DF micrograph of a $Ca_{0.5}Sr_{0.5}O_{2.5}$ sample containing domains of size 100–300 Å. This is in agreement with the data on coherence length determined from X-ray diffraction data (Fig. 2c). SAED patterns of these samples contain, besides strong perovskite reflections of a definite zone, a number of low-intensity reflections filling the regions between strong reflections (Figs. 5b). The positions of these weak reflections with respect to a symmetrical net of strong reflections are regular, which means that the observed microdomains are in quite definite orientational relationship with the matrix. As a rule, reflections of low

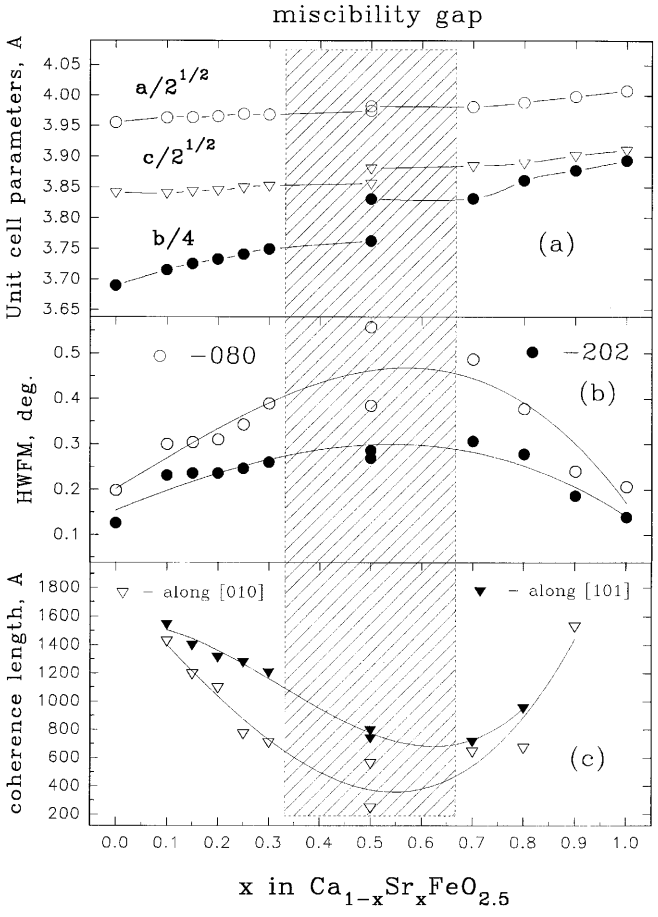

Fig. 2 X-ray diffraction data of $Ca_{1-x}Sr_xFeO_{2.5}$ samples: (*a*) change of reduced unit cell parameters with *x*; (*b*) variation of line width of the 080 and 202 reflections with *x*; (*c*) variation of the coherence length along the [010] and [101] directions with *x*

intensity exhibit diffuse streaking connected with diffraction on two-dimensional microdomain boundaries. Indexing of low-intensity reflections shows that the microdomains are related both to the phase close in

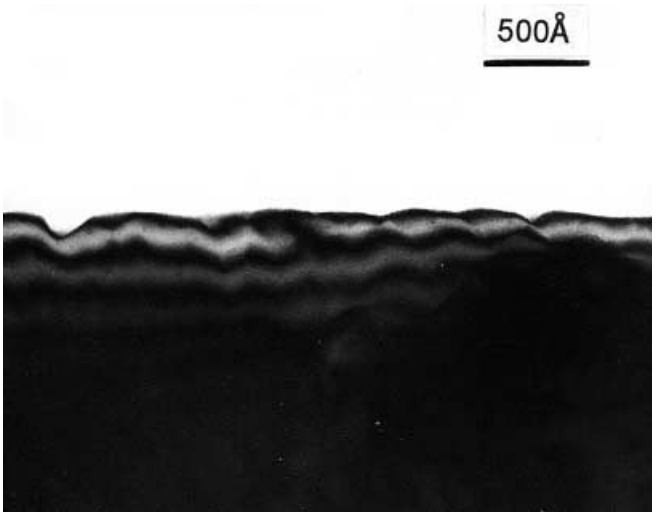

Fig. 3 Bright-field image of $CaFeO_{2.5}$ particle. The smooth thickness contours of the extinction point to the structural perfection of the crystal

structural parameters to $SrFeO_{2.5}$ and to the phase close to $CaFeO_{2.5}$, which is also in agreement with X-ray data.

For samples with nominal composition $Ca_{0.3}Sr_{0.7}FeO_{2.5}$, the size of the microdomains are much smaller (20–60 Å). They can be seen in the DF images of the crystals with thickness extinction contours (Fig. 6) which are not smooth like $CaFeO_{2.5}$ (compare Fig. 3) but fractured and spotted. Unfortunately, microdiffraction patterns do not contain any reflections from the observed microdomains because they are too fine. Thus, it was impossible to perform a phase analysis. In this case the size of the microdomains is outside the sensitivity range of the X-ray method, and the presence of microdomains is not revealed in the coherence length analysis of the diffraction patterns. As observed by the X-ray method, a coherence length of size

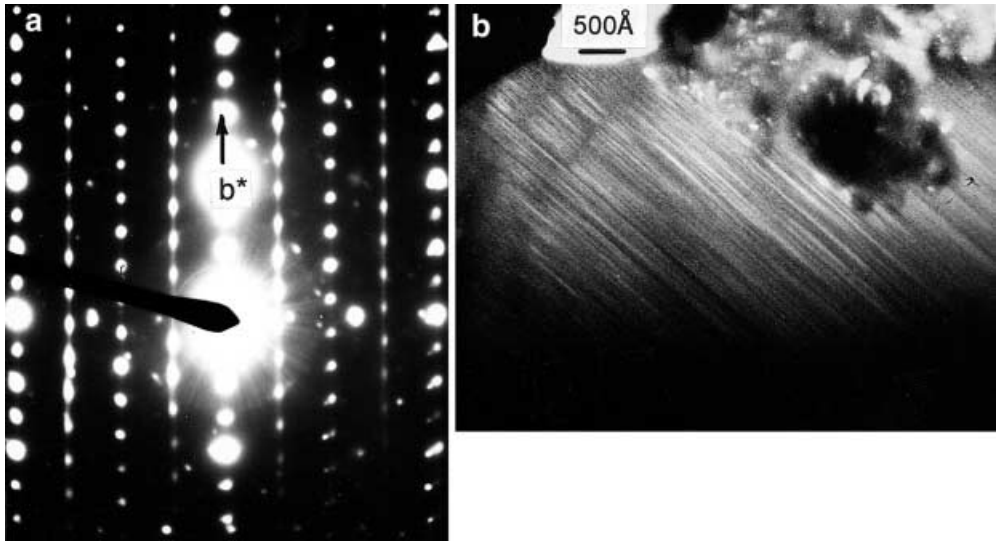

Fig. 4 **a** SAED picture of $SrFeO_{2.5}$ sample exhibiting streaking spots along the *b** direction. **b** Dark-field image of $SrFeO_{2.5}$ obtained in streaking reflection

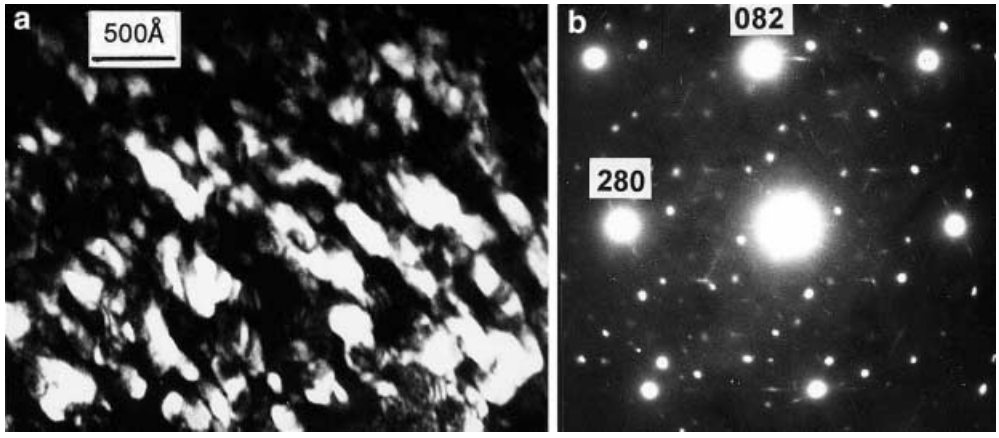

Fig. 5 **a** Dark-field image of the $Ca_{0.5}Sr_{0.5}FeO_{2.5}$ sample which represents the microdomain texture of the crystal. **b** SAED picture of the $Ca_{0.5}Sr_{0.5}FeO_{2.5}$ sample. *Strong reflections* are of the perovskite type. *Weak reflections* are stretched due to diffraction on the domain boundaries. They are related to the phases represented by solid solutions based on $SrFeO_{2.5}$ and $CaFeO_{2.5}$

600–800 Å is connected with the presence of grains in the samples.

For samples with nominal composition $Ca_{0.7}Sr_{0.3}FeO_{2.5}$, structure imperfections of two types are characteristic: the formation of grains of size 600–800 Å and the formation of very small cluster-like nuclei of size 20–30 Å or even smaller (Fig. 7). It can be assumed that the formation of these clusters is connected with the initial stages of phase separation.

Test of the reactivity of $Ca_{1-x}Sr_xFeO_{2.5}$ in electrochemical oxidation at room temperature

Sample oxidation was carried out in the galvanostatic mode at room temperature in 1 M KOH. Since the electronic conductivity of the samples decreases sharply with increasing Ca content, in order to achieve a constant current supply to the particles of the working electrode material, the latter was prepared with the addition of 15–20 wt% of acetylene black and 1 wt% of Teflon as a binding additive. The typical variations of the potential of the working electrode materials $Ca_{1-x}Sr_xFeO_{2.5}$ with the charge transfer (n) obtained in galvanostatic mode at a nominal current density of 1.5 μA/mg during the oxidation process are shown in Fig. 8. The studies showed that clear end points with quantitative conversion corresponding to Eq. 1:

$$Ca_{1-x}Sr_xFeO_{2.5} + 0.5O^{2-} \rightarrow Ca_{1-x}Sr_xFeO_{3.0} + e^- \quad (1)$$

at $n = 1e^-$/f.u. could be obtained for the samples with $x > 0.25$.

In the samples with $x < 0.25$ a strong overpotential arises at the initial stage of the oxidation. Oxygen evolution starts below the nominal charge transfer $n = 1e^-$/f.u. and no quantitative reaction is observed at $n = 1$ (the value calculated from Eq. 1). This is likely to be connected with substantial diffusion difficulties arising in oxygen transport into the working electrode material.

The results of iodometric titration of the samples obtained by galvanostatic oxidation ($n = 1e^-$/f.u.) are shown in Table 2. The deviation of oxygen content from the ideal composition at $0.25 < x < 1$ is connected with

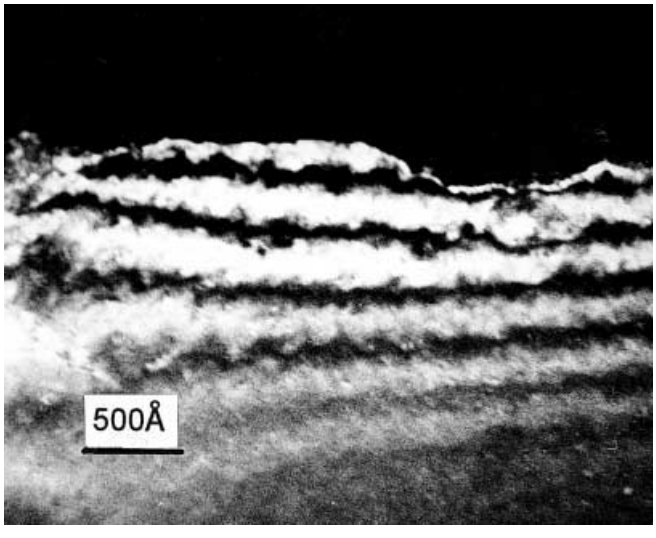

Fig. 6 Dark-field image of a $Ca_{0.3}$ $Sr_{0.7}FeO_{2.5}$ particle obtained in a strong perovskite-like reflection. *Bright contours* contain fractures and *spots* corresponding to microdomains with a size of 20–60 Å

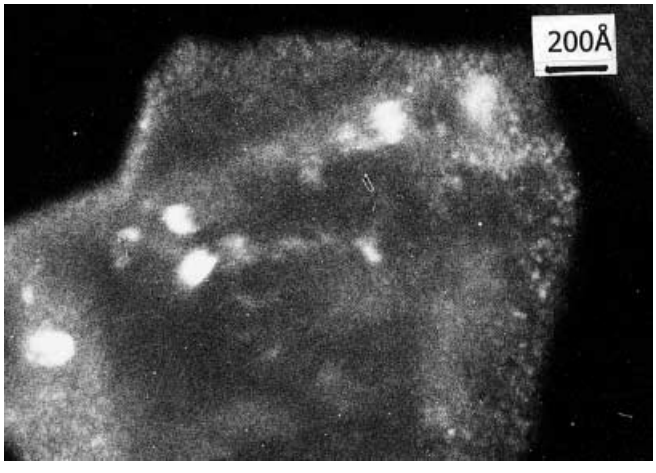

Fig. 7 Dark-field image of a $Ca_{0.7}Sr_{0.3}FeO_{2.5}$ particle which shows cluster-like nuclei about 20 Å in size

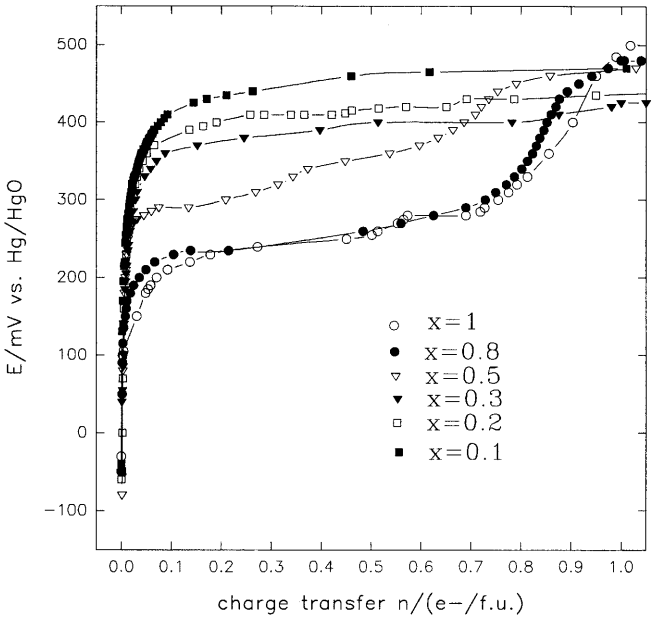

Fig. 8 Galvanostatic anodic oxidation of $Ca_{1-x}Sr_xFeO_{2.5}$ samples at room temperature in 1 M KOH electrolyte; change of potential E with charge transfer n

Table 2 Results of iodometric titration of $Ca_{1-x}Sr_xFeO_y$ after electrochemical oxidation with a charge transfer of $1e^-$/f.u

x	y
0.1	2.56(1)
0.15	2.61(1)
0.2	2.64(1)
0.25	2.94(1)
0.3	2.95(1)
0.5	2.94(1)
0.7	2.95(1)
0.8	2.97(1)
0.9	2.96(1)

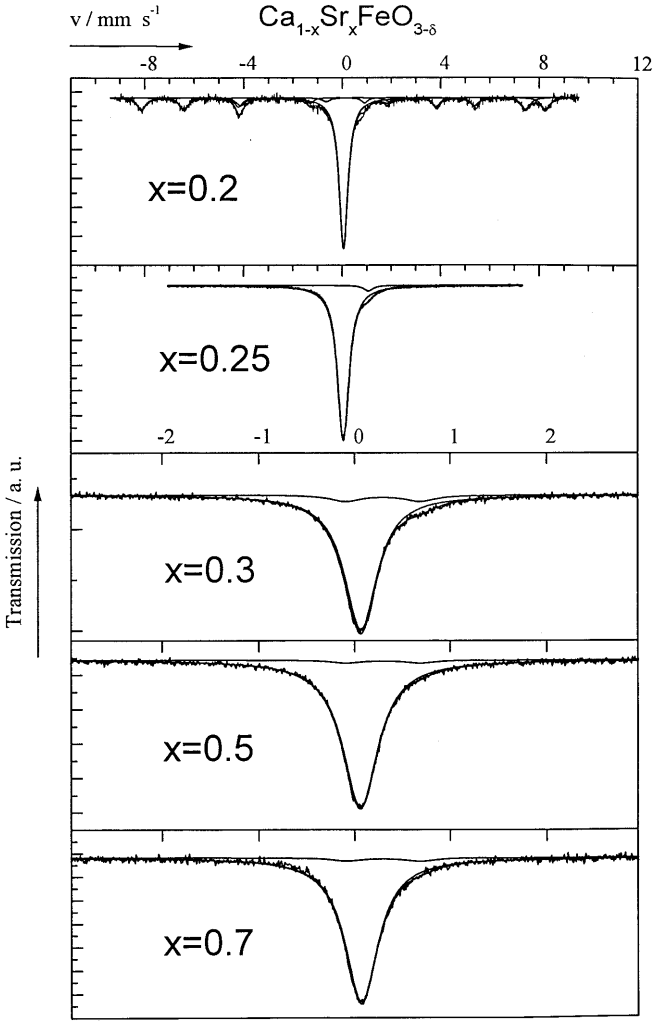

Fig. 9 Mössbauer spectra of electrochemically oxidized calcium-strontium ferrites

the low stability of these compounds owing to the high iron oxidation state. We have noted that the samples interact with water during washing and drying, resulting in water decomposition and oxygen gas evolution which is accompanied by a decrease in the oxygen content of the samples.

Mössbauer spectra of electrochemically oxidized samples with $x > 0.25$ (Fig. 9) show that 95–98% of iron ions have an oxidation state of $4+$ with similar δ and G parameters which equal 0.06 and 0.4, respectively. The doublet with integral intensity of 2–5% corresponds to Fe^{3+} and has $\delta = 0.31$, $G = 0.38$, $Q = 0.76$. Thus, iodometric and Mössbauer data confirm the bulk oxidation of the samples.

In the samples with $0 < x < 0.25$, the low oxygen content is mainly due to incomplete oxidation of $Ca_{1-x}Sr_xFeO_{2.5}$. This is in agreement with Mössbauer spectra, which exhibit the components corresponding to brownmillerite (Fig. 9).

Figure 10 presents the X-ray patterns of galvanostatically oxidized $Ca_{1-x}Sr_xFeO_{2.5}$ samples ($n = 1e^-$/f.u.). As Fig. 10 and Table 2 show, complete oxidation with the formation of cubic perovskite phases in the galvanostatic regime at $n = 1e^-$/f.u. is achieved for the compounds with $x \geq 0.25$. For the samples with $x = 0.3$ and 0.5, X-ray patterns contain two sets of cubic perovskite reflections. The ratio of their intensities is constant. This is due to an earlier-noted phase separation caused by the miscibility gap within the composition range $0.3 < x < 0.7$ and the formation of Ca- and Sr-enriched microdomains. The oxidation of these microdomains leads to the appearance of two sets of reflections related to Ca- and Sr-enriched cubic perovskite products. Since the oxidation of the samples with $x < 0.25$ was not completed at $n = 1e^-$/f.u., the X-ray patterns contain strong reflections of the parent brownmillerite compounds and weak cubic perovskite reflections (marked with arrows in Fig. 10) which are attributed to oxidation products. It should be noted that an increase in current density and/or the time of

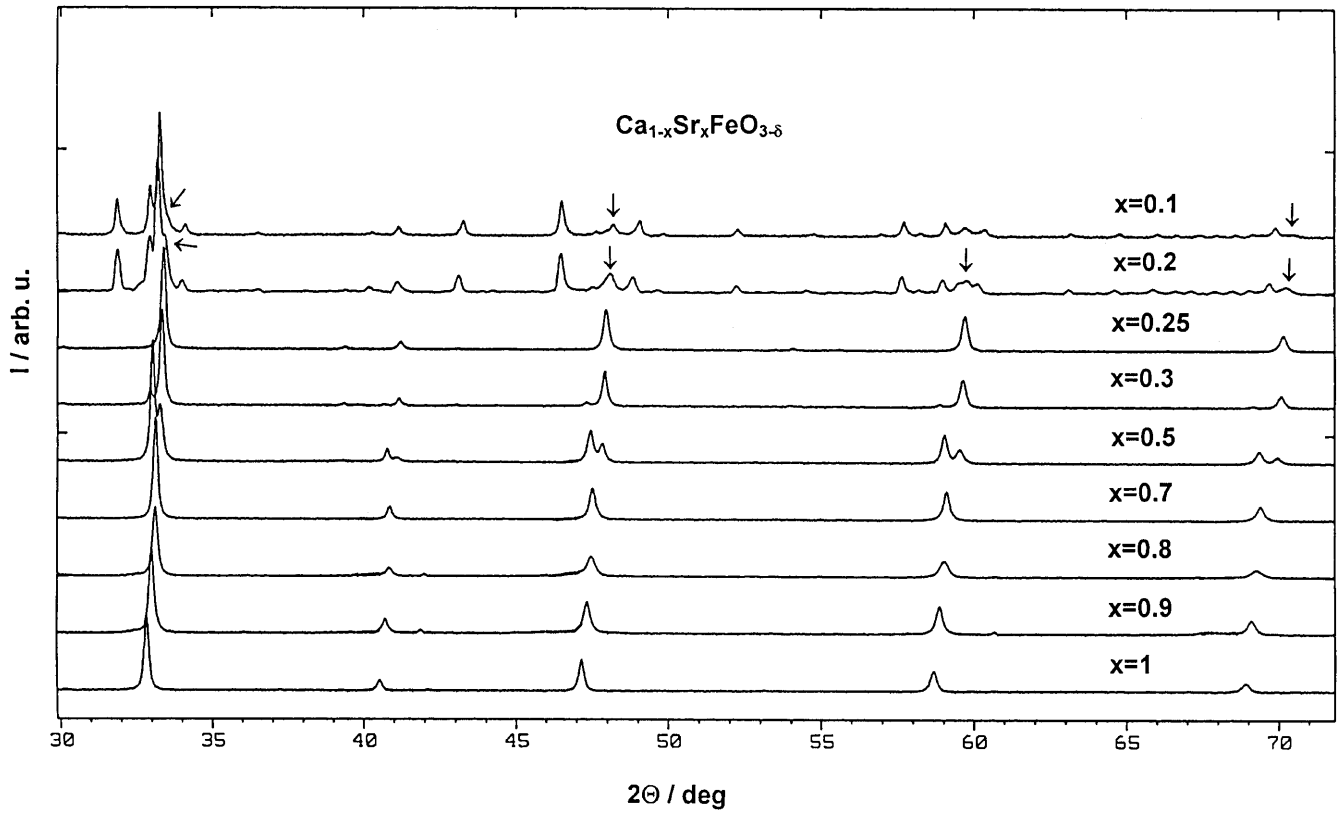

Fig. 10 X-ray diffraction patterns of calcium-strontium ferrites after electrochemical oxidation

electrochemical treatment of the samples with $x < 0.25$ did not lead to significant changes in the intensity of the cubic perovskite reflections or in the oxygen content. This means that the kinetics of the process slows down sharply and even at $n \gg 1$ a complete oxidation of the samples (in the volume) is not achieved within a reasonable time.

Figure 11 shows the results of the X-ray diffraction data evaluation on the basis of a cubic perovskite cell. A decrease in Sr content of the samples leads to a continuous decrease in the unit cell parameter. Within the range $0.3 < x < 0.7$, owing to the phase separation the formation of two types of products occurs. When the Ca content of the samples increases, the unit cell parameters of one of these products approach a value characteristic of pure $SrFeO_3$ and another to pure $CaFeO_3$. The calculations of the cubic unit cell parameters for the oxidation products of $Ca_{0.75}Sr_{0.25}FeO_{2.5}$ and $Ca_{1-x}Sr_xFeO_{2.5+y}$ ($x = 0.2$ and 0.1) samples show that they decrease further and approach the unit cell parameter for $CaFeO_3$, obtained by thermal synthesis in a girdle-type high-pressure apparatus at 1000 °C and $P_{O_2} = 2$ GPa [7]. For comparison, the available literature data on $CaFeO_3$ are shown in the plot. In one case, the structure of $CaFeO_3$ exhibited tetragonal distortions (black circles) [7, 9] and in the other case the structure was indexed as an ideal cubic perovskite (black square) [10].

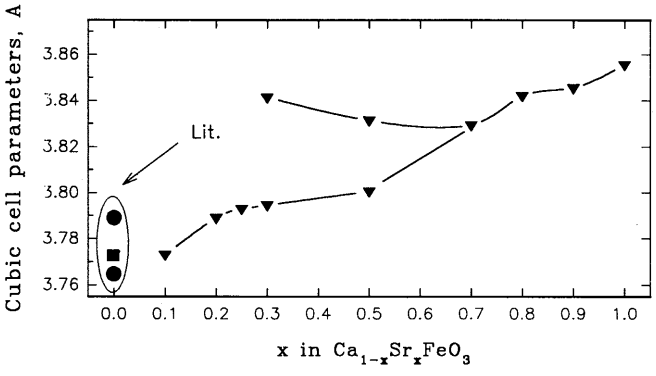

Fig. 11 X-ray diffraction data of calcium-strontium ferrites after electrochemical oxidation; change of perovskite cubic cell parameters with x

Discussion

On the basis of electron microscopy data, the initial $Ca_{1-x}Sr_xFeO_{2.5}$ samples are characterized by several kinds of imperfection. Twins and grains are characteristic of all the samples, and the obtained coherence length is likely to correlate with these defects. Besides, solid solutions of Ca in $SrFeO_{2.5}$ ($0.7 < x < 1$) inherit stacking faults which are characteristic of pure, unsubstituted $SrFeO_{2.5}$. However, in the background of the above-mentioned defects, an increase in Ca content is accompanied by the formation of microdomains connected with the unmixing of solid solutions. The

dimensions of the microdomains reach their maximum value (about 100–300 Å) at $x = 0.5$. In this case, it becomes possible to register the microdomains by X-ray diffraction, which leads to a noticeable broadening of the X-ray reflections. A drop in coherence length is determined in this case not by the size of twins or grains but by the size of the microdomains. A further increase in Ca content ($x < 0.3$) again causes a sharp decrease in the microdomain size. They become unregistered by X-ray diffraction. For $x = 0.3$, it is likely that electron microscopy images registered the initial stage of phase separation, frozen as a result of sample quenching in liquid N_2. The formation of microdomains within the range $0.7 < x < 1$ is connected with the formation of regions enriched with Ca within the crystal, while for $0 < x < 0.3$, regions enriched with Sr are formed which are more clearly manifested in the oxidation products (Figs. 10, 11). Thus, $Ca_{1-x}Sr_xFeO_{2.5}$ samples tend to the unmixing, with the microdomain formation similar to La/Ca ferrites studied earlier [11].

A comparison of EM data with the reactivity of samples in the course of electrochemical oxidation at room temperature leads to the conclusion that the major contribution to the reactivity increase is made by the microdomain formation. The presence of coarse twins and grains does not lead to an increase of the reactivity of the samples. In our opinion, electrochemical oxidation of the samples at room temperature occurs as a result of simplified oxygen diffusion along the extended defects (microdomains boundaries and stacking faults), followed by slow diffusion over short distances in the microdomains. A high concentration of low activation energy channels, the small size of the domains and the activity of oxygen formed during the anode oxidation of OH^- ions are conditions sufficient to provide the oxidation of not only the domains enriched with Sr but also Ca microdomains, even at room temperature within reasonable time intervals.

A decrease in Sr content of the samples at $x < 0.25$ causes stabilization of the solid solutions, inhibits phase separation, elevates the size of Ca-rich domains and the diffusion pathway inside them sharply, which causes an abrupt deceleration of the oxidation kinetics. As a result, the formation of small amounts of cubic perovskites observed by us at $x < 0.25$ is likely to be connected with the surface oxidation of coarse grains.

On the other hand, Sr-enriched microdomains and boundaries surrounding them can be described as a percolation network for fast oxygen transport within crystallites. From this point of view, a critical concentration of strontium $[Sr]_c = 25$ at% correlates with the percolation threshold for 3D structures [12].

It is interesting to note that the formation of $Ca_{1-x}Sr_xFeO_3$ was achieved earlier only by means of thermal synthesis in a girdle-type high-pressure apparatus at 1000 °C and $P_{O_2} = 2$ GPa [7]. An attempt at electrochemical oxidation of pure $CaFeO_{2.5}$ was unsuccessful [13]. This has been explained in terms of the high energy barrier for oxygen diffusion in the calcium compounds [13]. To explain fast oxygen diffusion in oxides concerned with the electrochemical oxidation at ambient temperature, it was assumed earlier that O^- species which might be formed via the charge transfer equilibrium:

$$M^{n+} + O^{2-} M^{(n-1)+} + O^- \quad (2)$$

participate in the oxygen diffusion process [14, 15]. However, there is no direct evidence so far that a transport mechanism of this kind is involved in the room temperature electrochemical oxidation discussed here. We have to take into account other factors that might explain the low-temperature oxygen transport phenomenon.

According to our results, one of essential factors for low oxygen transport in oxides is their microstructure; the combination of high concentrations of extended defects (e.g. dislocations, stacking faults, domain and anti-phase boundaries) with a low activation energy for oxygen mobility and the small size (10–10^2 Å) of defect-free domains may provide a relatively high overall rate of oxygen uptake. In spite of the high activation barrier for oxygen migration in calcium compounds, we succeeded in electrochemical oxidation of Ca microdomains, the reaction time being drastically decreased by short diffusion lengths.

Conclusion

The introduction of high concentrations of extended defects into $CaFeO_{2.5}$ by substitution with Sr leads to a sharp increase in the reactivity of the matrix; we performed electrochemical oxidation of the host lattice at room temperature. This confirms the phenomenological model proposed by us earlier, which describes an anomalous rapid (for such a low temperature) oxidation process in perovskites as a result of long-range fast oxygen transport along extended defect channels and slow diffusion over short distances in defect-free domains.

Acknowledgements This work has been supported by the Russian Foundation for Basic Research, grant N 00-03-32552a.

References

1. Wattiaux A, Fournes L, Demourgues A, Bernaben N, Grenier J-C, Pouchard M (1991) Solid State Commun 77:489
2. Bezdicka P, Wattiaux A, Grenier J-C, Pouchard M, Hagenmuller P (1993) Z Anorg Allg Chem 619:7
3. Nemudry A, Rudolf P, Schöllhorn R (1996) Chem Mater 8:2232
4. Nemudry A, Weiss M, Gainutdinov I, Boldyrev V, Schöllhorn R (1998) Chem Mater 10:2403
5. Goldberg E, Nemudry A, Boldyrev V, Schöllhorn R (1998) Solid State Ionics 110:223
6. Goldberg E, Nemudry A, Boldyrev V, Schöllhorn R (1999) Solid State Ionics 122:17
7. Takano M, Takeda Y (1983) Bull Inst Chem Res Kyoto Univ 61:406

8. Alario-Franco MA, Henche MJR, Vallet M, Calbet JMG, Grenier J-C, Wattiaux A, Hagenmüller P (1983) J Solid State Chem 46:23
9. Takeda Y, Naka S, Takano M, Shinio T, Takada T, Shimada M (1978) Mater Res Bull 13:61
10. Kanamaru F, Mijamoto H, Mimura Y, Koizumi M, Shimada M, Kume S, Shin S (1970) Mater Res Bull 5:257
11. Alario-Franco MA, Gonzalez-Calbet JM, Vallet-Regi M, Grenier J-C (1983) J Solid State Chem 49:219
12. Parsonage NG (1978) Disorder in crystals. Clarendon Press, Oxford
13. Grenier J-C, Doumerc J-P, Muraoka Y, Petit S, Pouchard M, Wattiaux A (1998) Solid State Ionics 108:9
14. Schöllhorn R (1988) Angew Chem Int Ed Engl 27:1392
15. Grenier J-C, Arrouy F, Locquet J-P, Monroux C, Pouchard M, Villesuzanne A, Wattiaux A (1994) The role of additional oxygen atoms on superconducting properties of La_2CuO_4-related compounds. In: Sigmund E, Müller K A (eds) Phase separation in cuprate superconductors. Springer, Berlin Heidelberg New York, pp 236–256